Author/s:
Catani, KJ;Muller, G;Da Silva, G;Bieske, EJ

Title:
Electronic spectrum and photodissociation chemistry of the linear methyl propargyl cation H2C4 H 3 +

Date:
2017-01-28

Citation:
Catani, K. J., Muller, G., Da Silva, G. & Bieske, E. J. (2017). Electronic spectrum and photodissociation chemistry of the linear methyl propargyl cation H2C4 H 3 +. Journal of Chemical Physics, 146 (4), https://doi.org/10.1063/1.4974338.

Persistent Link:
https://hdl.handle.net/11343/240891

# Electronic spectrum and photodissociation chemistry of the linear methyl propargyl cation $H_2C_4H_3^+$

Katherine J. Catani,[1] Giel Muller,[1] Gabriel da Silva,[2] and Evan J. Bieske[1, a)]

[1)] *School of Chemistry, The University of Melbourne, Victoria, Australia 3010*

[2)] *Department of Chemical and Biomolecular Engineering, The University of Melbourne, Victoria, Australia 3010*

(Dated: 7 January 2017)

The electronic spectrum of the methyl propargyl cation (2-butyn-1-yl cation, $H_2C_4H_3^+$) is measured over the 230–270 nm range by photodissociating the bare cation and its Ar and $N_2$ tagged complexes in a tandem mass spectrometer. The observed $^1A' \leftarrow {}^1A'$ band system has an origin at 37 753 $cm^{-1}$ for $H_2C_4H_3^+$, 37 738 $cm^{-1}$ for $H_2C_4H_3^+$-Ar , and 37 658 $cm^{-1}$ for $H_2C_4H_3^+$-$N_2$. The methyl propargyl cation photodissociates to produce either $C_2H_3^+ + C_2H_2$ (protonated acetylene + acetylene) or $H_2C_4H^+ + H_2$ (protonated diacetylene + dihydrogen). Photodissociation spectra of $H_2C_4H_3^+$, $H_2C_4H_3^+$-Ar and $H_2C_4H_3^+$-$N_2$ exhibit similar vibronic structure, with a strong progression of spacing 630 $cm^{-1}$, corresponding to excitation of the C-C stretch mode. Interpretation of the spectra is aided by ground and excited state calculations using time dependent density functional theory at the $\omega$B97X-D/aug-cc-pVDZ level of theory. *Ab initio* calculations and master equation simulations were used to interpret the dissociation of $H_2C_4H_3^+$ on the ground state manifold. These calculations support the experimentally observed product branching ratios in which acetylene elimination dominates and also suggests that channel switching occurs at higher energies to favor $H_2$ elimination.

[a)] Electronic mail: evanjb@unimelb.edu.au

## I. INTRODUCTION

Small carbocations including $C_3H_3^+$ and $C_4H_5^+$ are commonly observed in mass spectrometry and are important intermediates in organic chemical reactions, in combustion processes and in plasmas.[1–3] These hydrocarbon cations are also relevant from an astrophysical standpoint having been identified in the atmosphere of Titan and possibly existing in interstellar clouds.[4] Alkynyl type carbocations, such as $C_4H_5^+$, were originally observed in super-acidic media using NMR,[5–8] with subsequent computational studies suggesting that the methyl cyclopropenyl cation (Fig. 1a) is the lowest energy isomer of $C_4H_5^+$, with the linear methyl propargyl cation, $H_2C_4H_3^+$ (Fig. 1d) lying ≈106 kJ/mol higher in energy.[9,10]

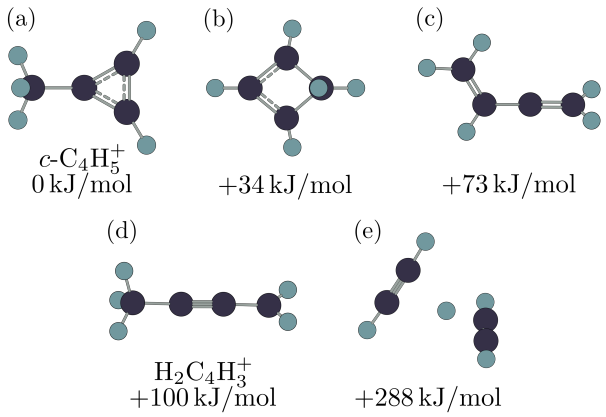


FIG. 1. Low-lying $C_4H_5^+$ isomers along with relative energies calculated at the MP2/aug-cc-pVDZ level.

Previously, there was limited spectroscopic data for the various $C_4H_5^+$ isomers in the gas phase that could serve as the basis for their detection. Duncan and coworkers measured an IR spectrum of the protonated dimer of acetylene, a form of $C_4H_5^+$ in which a proton is

attached to the $\pi$ cloud of both acetylene molecules, and which lies considerably higher in energy than the methyl cyclopropane (by 312 kJ/mol) and methyl propargyl cations.[11] In other related work, Lang et *al.* measured a threshold photoelectron spectrum of the neutral 2-butyn-1-yl radical, determining its adiabatic ionization energy and observing vibrational structure, which on the basis of a Franck-Condon analysis, was assigned to the C−C single bond stretch modes and the C≡C stretch mode of the $H_2C_4H_3^+$ cation.[12]

Likewise, there is limited data related to the decomposition pathways for $C_4H_5^+$. Following photoexcitation at 193 nm, the $H_2C_4H_3^+$ cation produced a charged photoproduct at $m/z$ 27, almost certainly protonated acetylene ($C_2H_3^+$).[13] Collision induced dissociation of $H_2C_4H_3^+$ also produced $C_2H_3^+$ through a process that was postulated to involve cyclization prior to fragmentation.[10] Recently Pei and Farrar investigated reactive collisions between $C^+$ and $C_3H_5$, which occur on the $C_4H_5^+$ potential energy surface, using velocity map imaging to probe the energy disposal in the reaction.[14] At significantly higher energy than for the other studies, they observed mainly $H_2$ loss from $C_4H_5^+$.

In the present study we have measured the $^1A' \leftarrow {}^1A'$ electronic spectrum of $H_2C_4H_3^+$ over the 230–270 nm range by monitoring the photodissociation products in a tandem mass spectrometer. Spectra recorded for the bare $H_2C_4H_3^+$ cation and the $H_2C_4H_3^+$-Ar, and $H_2C_4H_3^+$-$N_2$ complexes each exhibit well resolved vibronic bands, enabling us to make comparisons with predictions from electronic structure calculations and to unambiguously identify the carrier as the $H_2C_4H_3^+$ methyl propargyl cation. In conjunction with the spectroscopic measurements we have determined energies and structures for various $C_4H_5^+$ isomers and transition states through quantum chemical calculations, and have used statistical rate theory to predict the branching ratio for photodissociation of $H_2C_4H_3^+$ into the $C_2H_3^+ + C_2H_2$ and $C_4H_3^+ + H_2$ channels. These predictions are compared with the branching ratios observed following excitation of the $^1A' \leftarrow {}^1A'$ transition of $H_2C_4H_3^+$.

## II. EXPERIMENTAL APPROACH

The $^1A' \leftarrow {}^1A'$ electronic spectrum of $H_2C_4H_3^+$ was recorded by resonance-enhanced photodissociation of the bare $H_2C_4H_3^+$ cation and the $H_2C_4H_3^+$-Ar and $H_2C_4H_3^+$-$N_2$ complexes. The experimental arrangement has been described elsewhere,[15–18] and here only a brief outline is provided. Vapour from liquid 1-bromo-2-butyne ($C_4H_5Br$, 99% pure, Sigma Aldrich)

at room temperature, was seeded into a pulsed supersonic expansion of either argon or nitrogen gas (backing pressure 4 bar). The expanding gas was bombarded with electrons to form the closed-shell $H_2C_4H_3^+$ cation and the $H_2C_4H_3^+$-Ar or $H_2C_4H_3^+$-$N_2$ complexes. The target cations were mass-selected by a quadrupole mass filter and then deflected 90° by a quadrupole bender into an octopole ion guide where they were irradiated with light from a tuneable optical parametric oscillator (OPO, EKSPLA NT342B) with a bandwidth of $\approx$8 $cm^{-1}$ and pulse duration of 3-5 ns. Resonant photoexcitation of $H_2C_4H_3^+$ generated $H_2C_4H^+$ and $C_2H_3^+$ photofragments that were mass-selected by a second quadrupole mass filter and detected by a microchannel plate. The $H_2C_4H_3^+$-Ar and $H_2C_4H_3^+$-$N_2$ complexes produced $H_2C_4H_3^+$, $H_2C_4H^+$, and $C_2H_3^+$ photofragments in proportions that depended on wavelength. The photofragment ion signal was monitored as the laser wavelength was scanned to record a photodissociation action spectrum, which was subsequently normalised with respect to laser power. A wavemeter (Ångstrom LSA UVL) was used for wavelength calibration.

## III. COMPUTATIONAL APPROACH

According to previous computational studies, the $C_4H_5^+$ cation exists as several low-lying isomers separated by substantial interconversion barriers.[9,11] As part of this study, several of the more stable $C_4H_5^+$ isomers were investigated computationally along with the $C_4H_3^+$, $H_2$, $C_2H_3^+$, and $C_2H_2$ fragments. Density functional theory (DFT) methods, including $\omega$B97X-D[19] and CAM-B3LYP[20] with cc-pVDZ and aug-cc-pVDZ basis sets were used to determine ground state energies, geometric parameters, and harmonic frequencies. Excited states of $H_2C_4H_3^+$ were characterized using time dependent density functional theory (TD-DFT) with both CAM-B3LYP/cc-pVDZ and $\omega$B97X-D/aug-cc-pVDZ methods to determine the vertical and adiabatic excitation energies as well as the excited state harmonic frequencies. $H_2C_4H_3^+$ was optimised in the $C_s$ point group, and the ground and excited state vibrational frequencies were ordered based on their symmetries using the Mulliken convention.[21]

Structures and vibrational frequencies of the $H_2C_4H_3^+$-Ar and $H_2C_4H_3^+$-$N_2$ complexes were characterized employing DFT with the $\omega$B97X-D functional and aug-cc-pVTZ basis set. This level of theory, which incorporates empirical dispersion corrections, has been used for other charged non-covalently bound systems including quinoline$^+$-Ar and isoquinoline$^+$-Ar,[17]

indene$^+$-Ar,[18] indole$^+$-Ar,[22] $H_2C_3H^+$-$N_2$ and $H_2C_3H^+-Ne$.[23] All calculations were performed with the Gaussian 09 program suite.[24] Calculated vibrational frequencies of the complexes are provided in the Supplemental Material (Table S2).

Quantum chemical calculations conducted at the MP2/aug-cc-pVDZ level of theory were used to elucidate the $H_2C_4H^+ + H_2$ and $C_2H_3{}^+ + C_2H_2$ dissociation pathways with determination of structures and energies of relevant cationic and neutral fragments. Potential energy surfaces were scanned along bond lengths, rotations, and angles to identify minima and saddle points. The negative imaginary frequency for each transition state was visualised to ensure it corresponded to the correct transition along the reaction coordinate. In addition, the synchronous transit-guided quasi-newton (STQN)[25,26] method and intrinsic reaction coordinate (IRC)[27,28] calculations were used to find and verify saddle point geometries.

Statistical reaction rate theory simulations of energised $C_4H_5{}^+$ dissociation on the ground state potential energy surface were carried out within the MultiWell program suite,[29–31] using the MP2/aug-cc-pVDZ structures, vibrational frequencies, and energies. Stationary points were treated using the Rigid-Rotor-Harmonic-Oscillator approximations, with Stein-Rabinovitch-Beyer-Swinehart counts for sums and densities of states and RRKM theory for microscopic $k(E)$ values. For barrierless reactions the restricted Gorin model[32] was used to construct pseudo-transition state structures, adjusted so as to reproduce the Langevin theory rate coefficients for ion-molecule recombination. Time-dependent master equation simulations featured 3000 energy grains of $10\,\mathrm{cm}^{-1}$ width, after which the quasi-continuum regime was extended up to $200\,000\,\mathrm{cm}^{-1}$. Energy transfer to the bath gas was modelled using a single exponential-down model with $\Delta E_d$ of $200\,\mathrm{cm}^{-1}$ and estimated Lennard-Jones collision frequencies. Note that these parameters are of little consequence given the effectively collisionless regime of the experiments. So as to reproduce conditions within the octopole section of the instrument, simulations were carried out for $5\times10^{-8}$ Torr of Ar with a Boltzmann energy distribution at 30 K, the estimated vibrational energy of the ions, offset by the absorbed photon energy. Reported results represent fragment yields averaged over $10^6$ independent trajectories.

## IV. RESULTS AND DISCUSSION

### A. $^1A'\leftarrow{}^1A'$ spectra of $H_2C_4H_3^+$, $H_2C_4H_3^+$-Ar and $H_2C_4H_3^+$-$N_2$

The $^1A'\leftarrow{}^1A'$ resonance enhanced photodissociation spectra of $H_2C_4H_3^+$, $H_2C_4H_3^+$-Ar and $H_2C_4H_3^+$-$N_2$, recorded over the 230–270 nm range by monitoring $C_2H_3^+$ photofragments ($C_2H_2$ loss), are shown in Figure 2a, c and d. Measured band positions are given in the Supplemental Material (Table S1). The spectra are very similar and are dominated by an extended progression with a 630 $cm^{-1}$ spacing. The origin transition occurs at 37 753 $cm^{-1}$ for $H_2C_4H_3^+$, 37 738 $cm^{-1}$ for $H_2C_4H_3^+$-Ar (15 $cm^{-1}$ red shift), and 37 658 $cm^{-1}$ for $H_2C_4H_3^+$-$N_2$ (95 $cm^{-1}$ red shift). Almost identical, albeit weaker, action spectra were obtained in each case by monitoring $H_2C_4H^+$ photofragments ($H_2$ loss). For example, the spectrum of the bare $H_2C_4H_3^+$ cation recorded by monitoring $H_2C_4H^+$ is shown in Figure 2b. Spectra for $H_2C_4H_3^+$-Ar and $H_2C_4H_3^+$-$N_2$, obtained by monitoring the $H_2C_4H_3^+$ channel (i.e. loss of Ar or $N_2$, respectively), exhibit distinctly different relative peak intensities (comparison spectra are given in the Supplemental Material in Figures S2 and S3). Specifically, for $H_2C_4H_3^+$-Ar only the $11_0^1$ transition was observed when monitoring the $H_2C_4H_3^+$ photofragment. For the $H_2C_4H_3^+$-$N_2$ complex, the $H_2C_4H_3^+$ fragment signal diminished below 250 nm. The wavelength dependence of the $H_2C_4H_3^+$, $H_2C_4H^+$ and $C_2H_3^+$ photofragment intensities is discussed further in section IV C.

### B. Band Assignments

Initially, the $H_2C_4H_3^+$ $^1A'\leftarrow{}^1A'$ spectrum can be assigned in analogy to the spectrum of $H_2C_3H^+$ (Figure 2e), which was recently measured using the same technique.[23] Notably, there is only a slight shift of the $H_2C_4H_3^+$ origin to higher energy with respect to the $H_2C_3H^+$ origin, and the main progression has the same spacing (630 $cm^{-1}$) in the two spectra.[23] These observations imply that $H_2C_4H_3^+$ and $H_2C_3H^+$ are structurally similar with an acetylenic hydrogen atom replaced by a methyl group. For $H_2C_3H^+$ the dominant progression was assigned to the C-C stretch vibrational mode, $\nu_5$, with Franck-Condon activity associated with a lengthening of the C-C bond in the excited state.[23] Although the methyl group has little effect on the main C-C stretch progression, it does give rise to other progressions that contribute to spectral congestion.

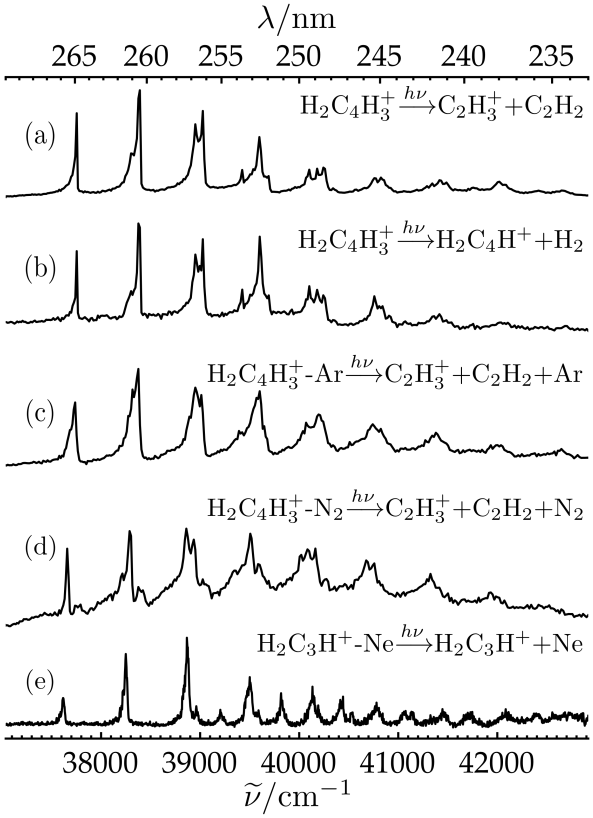


FIG. 2. $^1A' \leftarrow ^1A'$ spectra of: (a) $H_2C_4H_3^+$ recorded by monitoring $C_2H_3^+$; (b) $H_2C_4H_3^+$ recorded by monitoring $H_2C_4H^+$; (c) $H_2C_4H_3^+$-Ar recorded by monitoring $C_2H_3^+$; (d) $H_2C_4H_3^+$-$N_2$ recorded by monitoring $C_2H_3^+$. (e) Spectrum of $H_2C_3H^+$-Ne recorded by monitoring $H_2C_3H^+$ as reported in ref. 23.

To further understand the vibronic structure of the $H_2C_4H_3^+$ spectrum we conducted DFT and TD-DFT $\omega$B97X-D/aug-cc-pVDZ calculations for structures and vibrational frequencies in the ground and excited states (computed frequencies are summarized in Table S2 in the Supplemental Material). Initial simulations of the spectrum using PGOPHER[33] (Figures S5 and S6, Supplemental Material) indicated that the main progression was due to the $\nu_{11}$ C-C stretch mode but that its frequency was substantially overestimated. A similar situation was found for $H_2C_3H^+$, where TD-DFT calculations at several different levels of theory and basis sets significantly overestimated the excited state C-C stretch vibrational frequency (by $\approx$300 $cm^{-1}$).[23] However, higher order MCSCF and coupled cluster response methods reproduced the structural changes from the ground to excited state (0.16-0.19 Å,

C-C bond elongation), and predicted a vibrational frequency that overestimated the experimental value by only 56 $cm^{-1}$.[23] Because of computational cost, these higher level methods are not feasible for the larger $H_2C_4H_3^+$ system. Therefore, we simulated the $H_2C_4H_3^+$ spectrum using adjusted excited state vibrational frequencies, with the C-C stretch mode frequency $\nu_{11}$ scaled by 0.85 and other frequencies scaled by 0.957 (see Figures S5 and S6 in the Supplemental Material). As shown in Figure 3, there is a reasonably good match between experimental and simulated spectra, although the calculations predict a somewhat shorter $11_0^n$ progression than observed experimentally, suggesting that the C-C bond elongation in the excited state exceeds the calculated value (0.10 Å).

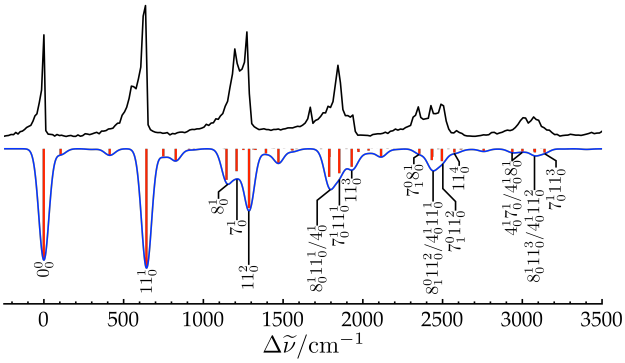


FIG. 3. Comparison of measured and simulated $^1A'\leftarrow{}^1A'$ spectra of $H_2C_4H_3^+$. The experimental spectrum is reproduced from Figure 2a while the simulated spectrum is constructed using PGOPHER based on DFT and TD-DFT ωB97X-D/aug-cc-pVDZ calculations, with the $\nu_{11}$ frequency scaled by 0.85 and other frequencies scaled by 0.957. A more comprehensively assigned spectrum is provided in the Supplemental Material (Figure S7).

The $H_2C_4H_3^+$ spectrum exhibits other weaker features, including the $7_0^1$ transition (out-of-phase $CH_3$ umbrella and C-C stretch) at $0_0^0$+1199 $cm^{-1}$, which occurs ≈65 $cm^{-1}$ below the calculated interval of 1264 $cm^{-1}$, a 5% difference. Blended into the same peak at $0_0^0$+1199 $cm^{-1}$ is a contribution from the $8_0^1$ transition (in-phase $CH_3$ umbrella and C−C stretch). Both the $7_0^1 11_0^n$ and $8_0^1 11_0^n$ progressions extend to at least $n$=4. There is a well resolved transition at about $0_0^0$+1672 $cm^{-1}$ in each of the experimental spectra that is not immediately predicted by the Franck-Condon simulations. This transition is most convincingly assigned as $4_0^1$ (C≡C stretch), which is predicted to occur at $0_0^0$+1872 $cm^{-1}$, exceeding the experimental interval by ≈200 $cm^{-1}$ or 12%. The $5_0^1$ or $6_0^1$ transitions are predicted to

lie too low in frequency (unscaled excited state values of 1413 and 1388 $cm^{-1}$, respectively) and are predicted to be relatively weak. A less likely alternative is that the band is due to $\nu_3$ ($CH_3$ symmetric stretch), which has a much larger calculated frequency of 2892 $cm^{-1}$. The transition could also conceivably correspond to two quanta of an $a''$ vibrational mode with a frequency of ≈836 $cm^{-1}$ in the excited state with the most probable candidate, based on calculated frequencies, being $\nu_{18}$ ($CH_2$ and $CH_3$ symmetric wag). However, the calculated excited state frequency is 956 $cm^{-1}$, about 120 $cm^{-1}$ or 14% too high. Furthermore, there is only a modest reduction of the calculated frequency from the ground state to the excited state (1003 to 956 $cm^{-1}$) so that the $18_0^2$ transition should be weak. Therefore, as stated above, the $0_0^0$+1672 $cm^{-1}$ band is most likely to be the $4_0^1$ transition.

### C. Photodissociation of $H_2C_4H_3^+$

The photodissociation mechanism for $H_2C_4H_3^+$ is not yet fully understood. The fact that $H_2C_4H_3^+$ dissociates to produce $C_2H_3^+$ and $H_2C_4H^+$ fragment ions following $^1A' \leftarrow ^1A'$ excitation suggests that at least some fraction of the molecules undergoes non-radiative decay, either internal conversion followed by dissociation on the ground state surface, or by coupling to a dissociative state. We consider it unlikely that $H_2C_4H_3^+$ requires more than a single photon to dissociate, as the photodissociation spectra were obtained using an unfocused light beam with modest energy flux (≤0.2 mJ/$cm^2$/pulse). Furthermore, the calculations described below (Section IV D) indicate that single photon excitation of its origin transition provides $H_2C_4H_3^+$ with sufficient energy to access the $C_2H_3^+ + C_2H_2$ and $H_2C_4H^+ + H_2$ dissociation channels (assuming nonradiative decay to the ground state surface). Another indication that dissociation of $H_2C_4H_3^+$ proceeds following absorption of a single photon is that the $H_2C_4H_3^+$-Ar and $H_2C_4H_3^+$-$N_2$ complexes mainly produced $C_2H_3^+$ photofragment ions rather than simply losing the Ar or $N_2$ tag, as would be expected, for example, if electronic excitation was followed by fluorescence to vibrationally excited levels of the ground electronic state.

An interesting aspect is that $H_2C_4H_3^+$ photodissociates to produce both $C_2H_3^+$ and $H_2C_4H^+$ fragment ions with the former fragment being favoured by a factor of ≈5, despite the $C_2H_3^+ + C_2H_2$ limit being calculated to lie 1.03 eV above the $H_2C_4H^+ + H_2$ limit. If the dissociation proceeds on the ground state surface this would suggest that there is a

larger barrier for the $H_2C_4H_3^+ \rightarrow H_2C_4H^+ + H_2$ channel than for the $H_2C_4H_3^+ \rightarrow C_2H_3^+ + C_2H_2$ channel. Details of the potential energy surface appropriate for the dissociation of $H_2C_4H_3^+$ and an explanation for the observed product branching ratios are developed below in Section IV D.

Tagging $H_2C_4H_3^+$ with an Ar atom has little influence on the branching ratios for production of $H_2C_4H^+$ and $C_2H_3^+$ products and the Ar atom seems to be a spectator (see Figure S2 in the Supplemental Material). The $H_2C_4H_3^+$ fragment (Ar loss channel) was observed in minor quantities for excitation of the $11_0^1$ transition but was difficult to detect at other wavelengths. In contrast, the $N_2$ tag markedly affects the photofragment branching ratios (see Figure S3 in the Supplemental Material). In the lower energy regions of the spectrum the $N_2$ molecule suppresses formation of $H_2C_4H^+$ compared to $C_2H_3^+$, while the $H_2C_4H_3^+$ cation ($N_2$ loss) is also an appreciable fragment. However, at higher excitation energies, the branching ratio for formation of $H_2C_4H^+$ and $C_2H_3^+$ is similar to that for the bare molecules, while the $N_2$ loss channel becomes insignificant.

### D. Modelling the $H_2C_4H_3^+$dissociation

The mechanisms for $H_2$ and $C_2H_2$ elimination from $H_2C_4H_3^+$, assuming the reaction proceeds on the ground surface, are discussed below. Figure 4 shows the key features of the ground state potential energy surface of $H_2C_4H_3^+$, representing the energetically preferable channels to dissociation. Portions of the isomerization pathways have been discussed in previous work by Cunje *et al.*[9] and Douberly *et al.*[11] in relation to the interconversion of $C_4H_5^+$. The extended surface resulting from this study is given in the Supplemental Material as Figure S9, with structural and energetic information provided in Figure S10 and Tables S3-S4.

*$H_2$ elimination.* The lowest-energy pathway to $H_2C_4H^+$ results from $H_2$-loss from the methyl group over a 2.59 eV barrier. Other pathways to dissociation were investigated, including 1,4-elimination of $H_2$ as recently proposed by Pei and Farrar,[14] however this route involves a calculated barrier of 3.58 eV and is much less competitive.

*$C_2H_2$ elimination.* The most energetically favourable dissociation channel involves acetylene loss to form protonated acetylene. All steps for this process require less energy than the 2.72 eV dissociation limit. Ground state neutral acetylene (singlet) was calculated to lie

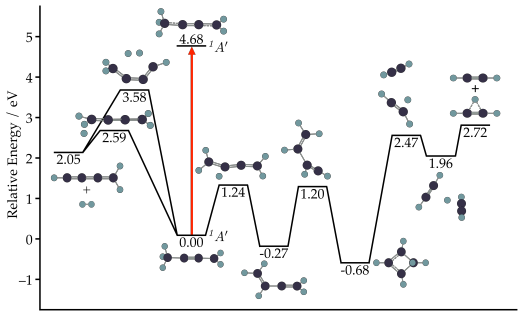


FIG. 4. Key features of the potential energy surface for $H_2C_4H_3^+$ dissociation to $H_2C_4H^+$ and $C_2H_3^+$ calculated at the MP2/aug-cc-pDVZ level. The $C_2H_2$ elimination channel involves multiple stationary points with lower energies than the dissociation limit of 2.72 eV; an extended surface is given in Figure S9 in the Supplemental Material. The excited $^1A'$ state energy (4.68 eV) corresponds to the experimental origin of the $^1A' \leftarrow {}^1A'$ transition.

2.03 eV lower in energy than vinylidene. This energy difference is consistent with previous experimental and theoretical investigations, which give values in the 1.86–2.04 eV range.[34–36] Therefore, it is unlikely that a vinylidene-loss pathway would be competitive within the wavelength range of the current experiment. Three $C_2H_3^+$ cation isomers were considered, including $H_3CC^+$, and the classical and bridged protonated acetylene cations. The $H_3CC^+$ structure is the least stable form, lying 2.21 eV above the most stable isomer, the non-classical, bridged protonated acetylene. Our MP2 calculations predict that the classical, vinyl $CHCH_2^+$ structure is a transition state.[37] However, higher level calculations suggest that the vinyl $CHCH_2^+$ cation is a stable structure lying 0.16 eV higher in energy than the non-classical cation from which it is separated by a tiny 0.005 eV barrier; this is probably insufficient to support a bound vibrational level.[37–40]

We have used RRKM theory / master equation simulations to model the dissociation of $H_2C_4H_3^+$ energized via electronic excitation followed by internal conversion to the ground state with 4.68 eV of additional internal energy (corresponding to excitation of the $^1A' \leftarrow {}^1A'$ origin transition). The model suggests that reaction proceeds entirely through the 2.47 eV transition state (for $C_2H_2$ loss) and the 2.59 eV transition state (for $H_2$ loss), even when the simulations are extended up to high energies (see below). At 4.68 eV the simulations

predict that $C_2H_3^+$+$C_2H_2$ accounts for 65% of the product yield under the experimental conditions, with the remaining 35% being $H_2C_4H^+$+$H_2$. We estimate an uncertainty of around 10kJ/mol (0.1 eV) in our barrier height calculations, and adjusting the key $H_2$ elimination barrier by this much results in predicted yields of between 50% and 78% for $C_2H_2$ elimination. Our modelling results are in relatively good agreement with the experimentally determined branching ratios (≈85% $C_2H_2$ elimination, ≈15% $H_2$ elimination), consistent with the hypothesis that dissociation transpires on the ground state manifold. They do, however, suggest a barrier for $H_2$ elimination that is somewhat further elevated relative to the $C_2H_2$ elimination pathway energies than predicted at the MP2 level. Another possibility is that $H_2C_4H_3^+$ converts back to the ground state surface through a conical intersection directing it to more stable isomers such as those depicted at -0.27 eV and -0.68 eV in Figure 4; in these instances the statistical reaction model predicts somewhat increased yields of $C_2H_3^+$.

The reaction model described above has been extended to predict the branching between $C_2H_3^+$ and $H_2C_4H^+$ ion products from $C_4H_5^+$ dissociation across a range of energies (Figure 5). The model conditions were kept the same as those used previously, and should be representative of any low temperature collision-free environment. Again, this assumes that reactions proceed entirely on the ground state and are initiated by the absorption of a single photon followed by internal conversion. At energies just above the threshold required to access both reaction channels, fragmentation to $C_2H_3^+$+$C_2H_2$ can be seen to dominate. At these energies the reaction flux bottleneck for acetylene elimination is the tight transition state at 2.47 eV, which is energetically favoured compared to the transition state for $H_2$ loss (2.59 eV). The predicted branching fractions are, however, very sensitive to the calculated barrier heights, given their similarities. The observation of exclusive $C_2H_3^+$ formation from the collision induced dissociation of $C_4H_5^+$ (Figure S1b of Lalli *et al.*)[10] – a low energy fragmentation process – once again supports a barrier for this reaction at the lower end of the expected range. At around 5.5 eV there is predicted to be a cross-over in product yields, with $C_4H_3^+$ becoming the dominant product ion. Subsequently, if the $C_4H_5^+$ cation is produced on the ground state surface in a highly vibrationally excited state (∼10 eV and above) then fragmentation is predicted to almost exclusively favour $C_4H_3^+$+$H_2$. This can explain the recent findings of Pei *et al.*,[14] where $C_4H_5^+$ produced from $C^+$ collisions with $C_3H_5$ were found to almost exclusively yield $C_4H_3^+$ product ions. Note that $H_2C_4H_3^+$ formation from

$C^+ + C_3H_5$ is around 10 eV exothermic, with the Pei *et al.* experiments conducted at collision energies of 2.2 eV.

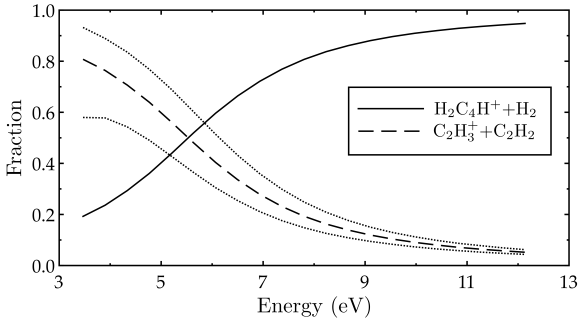


FIG. 5. Product branching fractions for $C_4H_5^+$ dissociation as a function excess internal energy from master equation simulations at 100 K with $5\times10^{-8}$ Torr of Ar gas. Dotted lines indicate the effect of varying the barrier for $H_2$ elimination by $\pm10$ kJ mol$^{-1}$ on the fractional yield of $C_2H_3^+ + C_2H_2$.

## V. SUMMARY AND CONCLUSIONS

The $^1A' \leftarrow {}^1A'$ electronic spectrum of the methyl propargyl cation ($H_2C_4H_3^+$) has been measured over the 230–270 nm range by photodissociation of mass-selected ions in a tandem mass spectrometer. The dominant progression with a spacing of 630 cm$^{-1}$ has been assigned to the $\nu_{11}$ C-C stretch vibrational mode. Photodissociation mainly generates $C_2H_3^+ + C_2H_2$ fragments rather than $H_2C_4H^+ + H_2$ fragments due to a larger energy barrier for production of the latter products. The reaction model described here appears capable of reproducing the main features of ground state $C_4H_5^+$ dissociation across a range of energies, and predicts that this process exhibits channel-switching behaviour. This is consistent with existing experimental data for $H_2C_4H_3^+$ dissociation, with $C_2H_3^+$ favored as the ionic product at lower energies and $C_4H_3^+$ at higher energies. The complexities inherent in $H_2C_4H_3^+$ dissociation will need to be incorporated into reaction models featuring this species, recognizing that the reaction products may vary depending upon the way in which this species is formed.

## SUPPLEMENTAL MATERIAL

The supplemental material includes: (i) measured $^1A' \leftarrow ^1A'$ spectra of $H_2C_4H_3^+$, $H_2C_4H_3^+$-Ar and $H_2C_4H_3^+$-$N_2$ recorded by monitoring different charged photofragments; (ii) measured band positions and assignments; (iii) calculated vibrational frequencies for $H_2C_4H_3^+$; (iv) simulated $^1A' \leftarrow ^1A'$ spectra for $H_2C_4H_3^+$; (v) calculated structures for $H_2C_4H_3^+$-Ar and $H_2C_4H_3^+$-$N_2$; (vi) structures and energies for $C_4H_5^+$ species that play a role for the dissociation of $H_2C_4H_3^+$ into the $C_2H_3^+$+ $C_2H_2$ and $C_4H_3^+$+ $H_2$ channels.


## ACKNOWLEDGMENTS

This research was supported under the Australian Research Council's Discovery Project funding scheme (Project Numbers DP150101427 and DP160100474) and by the Australian Government Research Training Program Scholarships.


## REFERENCES


[1]J. M. Goodings, D. K. Bohme, and N. Chun-Wai, Combust. Flame **36**, 27 (1979).

[2]N. Hansen, S. J. Klippenstein, C. A. Taatjes, J. A. Miller, J. Wang, T. A. Cool, B. Yang, R. Yang, L. Wei, C. Huang, J. Wang, F. Qi, M. E. Law, and P. R. Westmoreland, J. Phys. Chem. A **110**, 3670 (2006).

[3]I. N. Kosarev, N. L. Aleksandrov, S. V. Kindysheva, S. M. Starikovskaia, and A. Y. Starikovskii, Combustion and Flame **156**, 221 (2009).

[4]J. H. Waite Jr., D. T. Young, T. E. Cravens, A. J. Coates, F. J. Crary, B. Magee, and J. Westlake, Science **316**, 870 (2007).

[5]C. U. Pittman Jr. and G. A. Olah, J. Am. Chem. Soc. **87**, 5632 (1965).

[6]H. G. Richey Jr., J. C. Philips, and L. E. Rennick, J. Am. Chem. Soc. **87**, 1381 (1965).

[7]H. G. Richey Jr., L. E. Rennick, A. S. Kushner, J. M. Richey, and J. C. Philips, J. Am. Chem. Soc. **87**, 4017 (1965).

[8]G. A. Olah, R. J. Spear, and P. W. Westerman, J. Am. Chem. Soc. **96**, 5855 (1974).

[9]A. Cunje, C. F. Rodriquez, M. H. Lien, and A. C. Hopkinson, J. Org. Chem. **61**, 5212 (1996).

[10]P. M. Lalli, Y. E. Corilo, P. V. Abdelnur, M. N. Eberlin, and K. K. Laali, Org. Biomol. Chem. **8**, 2580 (2010).

[11]G. E. Douberly, A. M. Ricks, B. W. Ticknor, W. C. McKee, P. v. R. Schleyer, and M. A. Duncan, J. Phys. Chem. A **112**, 1897 (2008).

[12]M. Lang, F. Holzmeier, P. Hemberger, and I. Fischer, J. Phys. Chem. A **119**, 3995 (2015).

[13]D. J. Beussman, T. A. Erickson, and C. G. Enke, J. Am. Soc. Mass Spectrom. **7**, 114 (1996).

[14]L. Pei and J. M. Farrar, J. Phys. Chem. A **120**, 6122 (2016).

[15]D. A. Wild and E. J. Bieske, Int. Rev. Phys. Chem. **22**, 129 (2003).

[16]V. Dryza, N. Chalyavi, J. A. Sanelli, and E. J. Bieske, J. Chem. Phys. **137**, 204304 (2012).

[17]V. Dryza, J. A. Sanelli, E. G. Robertson, and E. J. Bieske, J. Phys. Chem. A **116**, 4323 (2012).

[18]N. Chalyavi, V. Dryza, J. A. Sanelli, and E. J. Bieske, J. Chem. Phys. **138**, 224307 (2013).

[19]J. D. Chai and M. Head-Gordon, Phys. Chem. Chem. Phys. **10**, 6615 (2008).

[20]T. Yanai, D. P. Tew, and N. C. Handy, Chem. Phys. Lett. **393**, 51 (2004).

[21]R. S. Mulliken, J. Chem. Phys. **23**, 1997 (1955).

[22]N. Chalyavi, K. J. Catani, J. A. Sanelli, V. Dryza, and E. J. Bieske, Mol. Phys. **113**, 2086 (2015).

[23]K. J. Catani, J. A. Sanelli, V. Dryza, N. Gilka, P. R. Taylor, and E. J. Bieske, J. Chem. Phys. **143**, 184306 (2015).

[24]M. J. Frisch, G. W. Trucks, H. B. Schlegel, G. E. Scuseria, M. A. Robb, J. R. Cheeseman, G. Scalmani, V. Barone, B. Mennucci, G. A. Petersson, H. Nakatsuji, M. Caricato, X. Li, H. P. Hratchian, A. F. Izmaylov, J. Bloino, G. Zheng, J. L. Sonnenberg, M. Hada, M. Ehara, K. Toyota, R. Fukuda, J. Hasegawa, M. Ishida, T. Nakajima, Y. Honda, O. Kitao, H. Nakai, T. Vreven, J. A. Montgomery, Jr., J. E. Peralta, F. Ogliaro, M. Bearpark, J. J. Heyd, E. Brothers, K. N. Kudin, V. N. Staroverov, R. Kobayashi, J. Normand, K. Raghavachari, A. Rendell, J. C. Burant, S. S. Iyengar, J. Tomasi, M. Cossi, N. Rega, J. M. Millam, M. Klene, J. E. Knox, J. B. Cross, V. Bakken, C. Adamo, J. Jaramillo, R. Gomperts, R. E. Stratmann, O. Yazyev, A. J. Austin, R. Cammi, C. Pomelli, J. W. Ochterski, R. L. Martin, K. Morokuma, V. G. Zakrzewski, G. A. Voth, P. Salvador, J. J. Dannenberg, S. Dapprich, A. D. Daniels, Ö. Farkas, J. B. Foresman, J. V. Ortiz, J. Cioslowski, and D. J. Fox, "Gaussian 09 Revision A.1," Gaussian Inc. Wallingford CT

2009.

[25]C. Peng and B. Schlegel, J. Chem. Phys. **33**, 449 (1993).

[26]C. Peng, P. Y. Ayala, H. B. Schlegel, and M. J. Frisch, J. Comp. Chem. **17**, 49 (1996).

[27]K. Fukui, Acc. Chem. Res. **14**, 363 (1981).

[28]H. P. Hratchian and H. B. Schlegel, Theory and applications of computational chemistry: the first forty years **4**, 195 (2005).

[29]J. R. Barker, Inter. J. Chem. Kinet. **33**, 232 (2001).

[30]J. R. Barker, Inter. J. Chem. Kinet. **41**, 748 (2009).

[31]"MultiWell-2013 Software, 2013, designed and maintained by J.R. Barker with contributors N.F. Ortiz, J.M. Preses, L.L. Lohr, A. Maranzana, P.J. Stimac, T. L. Nguyen, and T. J. Dhilip Kumar, University of Michigan, Ann Arbor, MI; http://aoss.engin.umich.edu/multiwell/,".

[32]G. P. Smith and D. M. Golden, Inter. J. Chem. Kinet. **10**, 489 (1978).

[33]C. Western, "PGOPHER, a program for simulating rotational structure," (2010), University of Bristol, http://pgopher.chm.bris.ac.uk.

[34]N.-Y. Chang, M.-Y. Shen, and C.-H. Yu, J. Chem. Phys. **106**, 3242 (1997).

[35]J. F. Stanton and J. Gauss, J. Chem. Phys. **110**, 1831 (1999).

[36]S. Joseph and A. J. C. Varandas, J. Phys. Chem. A **14**, 13277 (2010).

[37]B. T. Psciuk, V. A. Benderskii, and H. B. Schlegel, Theor. Chem. Acc. **118**, 75 (2007).

[38]R. Lindh, J. E. Rice, and T. J. Lee, J. Chem. Phys. **94**, 8008 (1991).

[39]A. R. Sharma, J. Wu, B. J. Braams, S. Carter, R. Schneider, B. Shepler, and J. M. Bowman, J. Chem. Phys. **125**, 224306 (2006).

[40]R. K. Chaudhuri and K. F. Freed, J. Chem. Phys. **129**, 054308 (2008).